Dynamic biofilm architecture confers individual and collective mechanisms of viral protection

Lucia Vidakovic[1], **Praveen K. Singh**[1], **Raimo Hartmann**[1], **Carey D. Nadell**[1,3,*], and **Knut Drescher**[1,2,*]

[1]Max Planck Institute for Terrestrial Microbiology, D-35043 Marburg, Germany

[2] Department of Physics, Philipps University Marburg, D-35032 Marburg, Germany

[3]Department of Biological Sciences, Dartmouth College, Hanover, NH 03755, USA

In nature, bacteria primarily live in surface-attached, multicellular communities, termed biofilms[1–6]. In medical settings, biofilms cause devastating damage during chronic and acute infections; indeed, bacteria are often viewed as agents of human disease[7]. However, bacteria themselves suffer from diseases, most notably in the form of viral pathogens termed bacteriophages[8–12], which are the most abundant replicating entities on Earth. Phage-biofilm encounters are undoubtedly common in the environment, but the mechanisms that determine the outcome of these encounters are unknown. Using *Escherichia coli* biofilms and the lytic phage T7 as models, we discovered that an amyloid fiber network of CsgA (curli polymer) protects biofilms against phage attack *via* two separate mechanisms. First, collective cell protection results from inhibition of phage transport into the biofilm, which we demonstrate *in vivo* and *in vitro*. Second, CsgA fibers protect cells individually by coating their surface and binding phage particles, thereby preventing their attachment to the cell exterior. These insights into biofilm-phage interactions have broad-ranging implications for the design of phage applications in biotechnology, phage therapy, and the evolutionary dynamics of phages with their bacterial hosts.

There is a rich literature on the co-evolution of bacteria and their viruses[13–17], yet little is known about the interactions between biofilms and phages. While a number of studies have determined the outcome of biofilms exposed to phages[18–23], this work has not provided an understanding of the mechanisms that govern phage-biofilm interactions. To address this open question, we developed a method for visualizing infection and spread of lytic T7 phages in living *E. coli* biofilms at single-cell resolution (Supplementary Fig. 1).

Biofilm size, matrix composition, internal architecture, and cellular physiology can vary dramatically during biofilm growth[4,5,24], so we hypothesized that phage susceptibility may vary as a function of biofilm developmental stage. To test this possibility, biofilms of varying ages – grown in microfluidic flow chambers at room temperature (24-26°C) – were exposed to a continuous influx of phages and imaged by confocal microscopy every 30-60 min for 12 h. We discovered that biofilms that had grown for 48 h or less were rapidly eradicated as a result of phage exposure. By contrast, biofilms that had grown for 60 h or more were collectively protected from phage-mediated killing, with minimally detectable background infection (Fig. 1). For such biofilms, infected cells were rare, always located on the outer biofilm edges, and did not result in propagation of infection further into the biofilm interior. We confirmed that the protection of biofilms to phage exposure was not due to a shift to stationary phase (Supplementary Fig. 2a), nor was it due to mutations that rendered cells physiologically resistant, as the bacterial populations within 72-h old biofilms were still susceptible to phage killing after being dispersed and re-grown in liquid culture (Supplementary Fig. 2b). The emergence of collective phage protection after 60 h of biofilm growth therefore seems to rely on properties that are specific to biofilms.

The extracellular matrix is an essential and unique feature of biofilm communities, and we hypothesized that matrix structure might be implicated in phage protection. To understand the impact of the matrix on phage spread, we generated mutants lacking each of the *E. coli* matrix components: proteinaceous curli fibers, flagellar filaments, cellulose, poly-β-1,6-*N*-acetyl-D-glucosamine (PGA), colanic acid, and type 1 fimbriae[3]. Each of these single-gene knockout mutants was able to produce 3-dimensional communities that are held together by an extracellular matrix, and therefore, by definition, was able to form biofilms. Mature biofilms composed of mutants deficient in any one of these matrix components retained protection from phages, except for mutants lacking curli amyloid fibers (Fig. 2a). Biofilms lacking curli were quickly eradicated by phages (Fig. 2a, Supplementary Fig. 3). A curli operon (*csgBAC*) transcriptional reporter, together with visualization of secreted CsgA *via* immunofluorescence, confirmed that curli are produced predominantly in the upper region of biofilms (Fig. 2b,c), and that curli fibers localize in the space between cells, but also cover most cells on the biofilm outer edge (Supplementary Fig. 4). The curli localization in the upper regions of our flow chamber biofilms is consistent with previous reports[24,25]. Furthermore, curli production initiates between 48 and 60 h after the start of biofilm growth (Fig. 2b,c), corresponding exactly to when biofilms gain protection against phage infection. Biofilms produced by a strain harboring a *csgD* promoter mutation (termed *csgD**), which causes curli expression at earlier time points during biofilm growth[26], show a corresponding earlier shift from phage susceptibility to phage protection (Fig. 2d).

Transcriptional activity profiles of other matrix components were weak in comparison with that of curli, or did not correspond well in space and time with the emergence of phage protection (Fig. 2b, Supplementary Figs. 5,6). These results establish that bacteria residing within mature (60 h) biofilms are collectively protected from phage infection in a manner dependent on curli amyloid fibers within the extracellular matrix, while cells inside the biofilm remain physiologically susceptible to phages (Supplementary Fig. 2a,b). This is a novel strategy of phage infection avoidance, distinct from other mechanisms of phage immunity, such as CRISPR-Cas, restriction-modification, abortive infection, or alteration of

phage binding sites8. In analogous experiments using T5 phages instead of T7 phages, we observed an identical transition from phage susceptibility to protection as a function of biofilm age (Supplementary Fig. 7), suggesting that this mode of phage protection is generic to different kinds of bacterial viruses.

To understand how curli fibers confer phage protection, we investigated if the biofilm architecture changes upon curli production, and how such changes impact phage mobility inside biofilms. To track individual phages, we conjugated purified T7 virions to a fluorescent dye (Alexa Fluor 488). Labeled phages were then incubated with mature biofilms (72 h) of wild type *E. coli*, as well as each of the matrix mutants described above. For biofilms produced by wild type cells, or by mutants lacking PGA (*pgaC*), colanic acid (*wcaE*), or cellulose (*bcsA*), phages accumulated only on the outer biofilm periphery (Fig. 3a-d). Biofilms lacking curli fibers (*csgB*), by contrast, permitted phages to diffuse freely through their entire volume (Fig. 3e). Using recently developed single-cell resolution biofilm imaging techniques5, we discovered that cells inside biofilms lacking curli fibers were less densely packed (Fig. 3h) and displayed a high cell-cell alignment (Fig. 3i). Such a biofilm architecture generated pores between cells that were wide enough for the phages to diffuse into the biofilm.

Surprisingly, biofilms produced by cells lacking flagella (*fliC*) also permitted phage diffusion (Fig. 3g), without allowing phage infection (Fig. 2a). This observation suggests that there is a second mechanism of phage protection that is active even when phages have penetrated into the biofilm interior. To understand why the *fliC* biofilm architecture permits phage diffusion, we investigated this architecture at high resolution, finding cell- and curli-free regions into which the phages were able to diffuse (Supplementary Fig. 8). The presence of such unoccupied regions yields a biofilm architecture with a lower cell-cell-alignment and a distribution of local cell densities that is broader and shifted to lower values, compared with the wild type (Fig. 3h,i). Together with the data of the curli mutant discussed above, these results indicate that cell-cell spacing, rather than cell-cell alignment, is the key biofilm-architecture parameter that determines phage transport in biofilms.

To determine how the gaps in the biofilm architecture of *fliC* biofilms arise, we investigated the activity of the *fliC* and *csgBAC* promoters in biofilms. Consistent with previous reports of the inverse regulation of flagella and curli24,27,28, we found that in *fliC* biofilms, promoters of flagella and curli synthesis were both active, but never in the same cell (Supplementary Fig. 9a). A *fliC* biofilm therefore contains a fraction of cells that produce neither curli nor flagella (Supplementary Fig. 9a,b), resulting in cracks in the architecture that are exploited by phages (Supplementary Fig. 8). Interestingly, in biofilms of a strain lacking the flagellar master regulator FlhDC, nearly all cells in the biofilm produce curli (Supplementary Fig. 9c), which results in a dense cell packing inside the biofilm that phages cannot invade (Fig. 3f). The *fliC* and *flhDC* mutants show that flagella themselves are not directly required for mediating phage protection, but instead have an indirect effect via the impact of flagella regulation on curli production.

Our results thus far establish that curli fibers arrange biofilm architecture so as to prevent phage diffusion. However, it remains unclear whether the fibers themselves also prevent

phage diffusion through the pores between cells. To resolve this question, we constructed minimal synthetic biofilms composed of purified curli fibers and fluorescent micro-beads with a size similar to bacterial cells (1.0 μm diameter). Purified CsgA proteins, the monomers of curli fibers, spontaneously assemble into filaments, which then formed a 3D matrix when incubated on their own (Fig. 4a). Co-incubation of T7 phages and the preformed curli network resulted in binding of phages to the amyloid fibers, as verified by fluorescence and electron microscopy (Fig. 4b,c). However, the curli mesh by itself did not prevent the diffusion of phage virions (Fig. 4b). Clusters of beads incubated on their own also permitted diffusion of phages, due to the large pore size between close-packed beads (Fig. 4d). Remarkably, when beads were incubated with *in vitro* polymerized curli fibers, they spontaneously formed clusters embedded within the curli mesh, and each curli-embedded bead cluster – like a wild type biofilm – prevented the diffusion of phages into its inner volume (Fig. 4e). Electron microscopy revealed that curli fibers localize in the pore-space between beads (Fig. 4f) and can directly capture phage virions, implying that even a sparse distribution of curli fibers in the pores is sufficient to prevent phage diffusion through biofilm pores.

Because *fliC* biofilms permitted phage diffusion (Fig. 3g), but not overall phage infection (Fig. 2a), we hypothesized that curli fibers might additionally protect cells on an individual basis, a mechanism that might also take effect in planktonic cultures. Consistent with this idea, we found that when T7 phages were added to shaken liquid cultures of wild type or *csgB* cells, the planktonic wild type populations were indeed more protected from phage infection than *csgB* populations (Supplementary Fig. 10). Electron microscopy confirmed that self-produced curli fibers can cover individual cells in planktonic culture (Fig. 4g). Importantly, *E. coli* exhibits bi-stable expression of the *csgBAC* operon in planktonic culture26,28, and we therefore tested the possibility that in a wild type population, only those cells that produce and embed themselves in curli show higher survival, whereas non-producing cells become infected and lyse. We immunostained the curli fibers in a planktonic wild type population and exposed these cells to our engineered T7 phages. We found that cells completely covered by curli were protected from phage infection, as predicted, while neighboring daughter cells that were not producing curli became infected and lysed (Fig. 4h). Binding of phages to the surrounding curli fibers (Fig. 4b,c) is likely to also prevent phages from attaching to the host cell exterior, yet it remains an open question to which extent phages with different host-cell adsorption mechanisms are can be shielded by the curli mesh. Complete coverage of the cell exterior by curli fibers was necessary for T7 phage protection of planktonic cells; cells that were incompletely covered remained unprotected and became infected and lysed over time (Fig. 4i).

Bacterial biofilms are ubiquitous, complex structures with broad ecological and medical impact, and they play a central role in microbial ecology and natural history. Here we have demonstrated that amyloid fibers, which constitute only a single component of the *E. coli* extracellular matrix, re-organize biofilm architecture such that susceptible bacteria achieve protection on the individual and collective cell level from exposure to phages. Investigating the general relationship between biofilm matrix production and biofilm-phage interactions, as well as modifying the diffusivity and infectivity of phages in biofilms, are therefore important directions for developing the next generation of therapeutic phages, for editing

microbiomes, and for a fundamental understanding of phage-bacteria co-evolution in nature[13,29,30].

Methods

Bacterial strains

All strains used in this study are derivatives of *E. coli* strain AR311024 and are listed in Supplementary Table 1. Chromosomal modifications inside the *E. coli* genome were generated by lambda red recombineering. The scarless lambda red system was applied to construct chromosomal transcriptional reporter fusions, 6x-His tagged *csgA*, curli complementation, and curli overexpression strains. Transcriptional reporter fusions were constructed by inserting *mKate2* into the chromosome, either extending the native operon or creating an artificial operon. To complement the *csgB* mutant, *csgB* was inserted under control of its native promoter into the *attB* site of *E. coli*. All strains constitutively express a fluorescent protein under control of the *tac* promoter (with the operator deleted) inserted into the *attB* site of *E. coli*.

T7 phage modification

We engineered recombinant T7 phage using the T7select415-1 phage display system (Millipore) with standard molecular biology techniques. We cloned the *E. coli* codon-optimized *sfgfp* (superfolder green fluorescent protein) gene under the control of the strong T7 *phi10* promoter downstream of the T7select415-1 *10B* capsid gene20. Infected host cells produced sfGFP rapidly enough to clearly fluoresce in the green channel before subsequently lysing and releasing a cohort of viable progeny phages (Supplementary Fig. 1).

Growth and phage infection experiments in the plate reader

Bacterial growth under constant shaking was monitored using a shaking incubator plate reader (Tecan Spark 10M). Optical density and fluorescence intensity measurements were performed every 5 minutes. Bacteria were grown at 37°C, where curli fiber expression does not occur (Supplementary Fig. 1, Fig. 2, and references[31,32]). For cases in which curli production was to be induced among cells in liquid culture, the growth temperature was set to 28°C (Supplementary Figure 2c, Supplementary Fig. 10).

Biofilm growth in microfluidic channels

Bacteria were grown in LB medium overnight at 37°C and shaking at 250 rpm. The cells were washed and diluted 1:80 in 0.9 % NaCl, inoculated into polydimethylsiloxane microfluidic devices, and incubated in the channels for one hour at room temperature (24-26°C) to colonize the glass substratum. Syringes containing tryptone broth (10 g L^{-1}) were connected with polyethylene tubing to the inlets of the microfluidic chambers. Residual planktonic cells were then removed from the chamber by increasing the flow to 50 µl min^{-1} for 40 sec. The flow rate was then decreased to 0.1 µl min^{-1} for the remainder of experiments, and the microfluidic channels as well as the inflowing medium were kept at room temperature (24-26°C).

Bacteriophage amplification and purification

E. coli AR3110 was grown under shaking conditions at 37°C until OD_{600} = 1.0. T7 phages were added, and the culture was incubated for an additional 3 h for phage amplification. The lysate was filter-sterilized (0.22 μm pore size) and stored at 4°C. To generate fluorescent phage virions, further purification was necessary. After phage amplification, DNaseI was added to the culture lysate, which was then incubated for 30 minutes at 37°C. Following DNA digestion, NaCl was added to a final concentration of 0.5 M, and the lysate was incubated for 1 h at 4°C. Phages were separated from cell debris by centrifugation for 10 min at 8000 g (4°C). The supernatant containing T7 phages was filtered (pore size 0.22 μm); PEG_{6000} (10% final concentration) was added and phages were allowed to precipitate overnight at 4°C. After centrifugation for 15 min at 8000 g (4°C) the phages were suspended in phosphate-buffered saline (PBS). To obtain pure phage cultures, density gradient centrifugation (62.5 %-21 % CsCl) was performed overnight at 100,000 g, followed by dialysis against PBS. The resulting highly purified T7 phages were stored at 4°C.

Bacteriophage labelling with fluorescent dye

Purified phages (100 μl, 10^{12} PFU mL^{-1}) mixed with sodium carbonate (0.1 M final) were incubated with 0.1 mg Alexa Fluor 488 for 1 h at room temperature under continuous shaking. The reaction mixture was dialyzed against PBS to separate phages from unbound dye. Fluorescently labelled phages were stored at 4°C.

Phage-biofilm interaction experiments and analysis

E. coli biofilms were exposed to T7 phages after growth for a defined time at room temperature. Immediately after addition of T7 phages (10^6 PFU mL^{-1}) or T5 phages (10^9 PFU mL^{-1}) biofilms were imaged with a confocal microscope every 30-60 min for 12 h. Imaging was performed on a Zeiss Axio Observer Laser Scanning Microscope (LSM 880) and a Nikon Ti-Eclipse inverted microscope fitted with a Yokogawa spinning disk confocal unit. Image analysis was performed using ZEN2.1, NIS Elements and Matlab. Data derived from *E. coli* biofilms grown in one channel (for treatments with or without phage exposure) were collated and defined as one replicate.

Curli localization inside *E. coli* biofilms

In order to visualize curli inside bacterial biofilms, a strain of *E. coli* AR3110 was constructed harbouring a C-terminal 6x-His tagged *csgA*. For detection of CsgA in live samples, grown biofilms were incubated with anti-6x-His-Tag antibodies conjugated to Alexa Fluor 488 or Alexa Fluor 647 (Qiagen product no.: 35310 or 35370; final concentration 0.4 μg mL^{-1}). Incubation with antibodies continued during confocal imaging.

CsgA purification

CsgA was purified *via* affinity chromatography. *E. coli* Rosetta (DE3) was transformed with a pET plasmid containing *csgA* with a C-terminal 6x His-Tag. The cells were grown over night at 30°C in the presence of 0.05% lactose for protein expression. Cell lysis and protein purification were performed according to an established protocol33. For protein purification, a prepacked Ni-NTA column was used instead of resin. Successful protein purification was

verified by western blotting using an anti-6x-His antibody conjugated to Alexa Fluor 488 (Qiagen product no.: 35310). Electron microscopy was used to confirm the polymerization of purified CsgA into curli fibers.

In vitro biofilm reconstruction

For *in vitro* biofilm reconstruction, fluorescent beads (with 1% bovine serum albumin; BSA) were pelleted in order to create bead aggregates. Fractions of the pellet were inserted into microfluidic channels with a poly-L-lysine-coated surface and incubated with fluorescently labelled phages (10^8 PFU mL^{-1}) for 1 h under constant flow (1 μl min^{-1}). Curli fibers were allowed to polymerize from purified CsgA, and were stained with Congo red (4 mg mL^{-1}) for 1 h at room temperature. These stained, pre-polymerized fibers were then incubated with beads for 1 h under constant shaking in the presence of 1 % BSA. The curli-bead mixture was then inserted into a microfluidic channel containing a poly-L-lysine-coated surface. Finally, fluorescently labelled phages (10^8 PFU mL^{-1}) were inserted under constant flow (1 μl min^{-1}) for 1 h. Phage diffusion through the *in vitro* reconstructed biofilms was visualized *via* confocal microscopy.

Phage interaction with single cells

In order to study phage infection of single cells that are protected by curli, *E. coli* (expressing CsgA-His) was grown overnight in tryptone broth (10 g L^{-1}) at 28°C (250 rpm) for enhanced curli production. This overnight culture was then incubated with anti-6x-His-Tag antibodies conjugated to Alexa Fluor 488 (Qiagen product no.:35310; final concentration 0.4 μg mL^{-1}). This suspension was inserted into microfluidic channels with a poly-L-lysine-coated surface. Finally, single cells were incubated with engineered T7 phages for 1 h under constant flow (0.2 μl min^{-1}).

In order to separate the sfGFP signal (indicating phage infection) from Alexa Fluor 488 signal (CsgA label), a custom Matlab script was used. If the green fluorescence signal overlapped with the red constitutive signal from the cell, the signal was interpreted to indicate phage infection reporter activity, and was displayed in cyan. If the green fluorescence signal did not overlap with the constitutive signal from the cell, the signal was interpreted to originate from Alexa Fluor 488 and indicate the presence of curli.

Biofilm architecture characterization at single-cell level

To investigate biofilm architectural properties at the single cell level, biofilms were imaged and segmented as described previously[5]. Unlike in the previous study, segmentation of cells in the biofilm was performed using a 3D edge detection algorithm, instead of thresholding single *z*-planes. Clumped structures were individualized by watershedding and/or *k*-means clustering. Local nematic order and cell density were calculated per cell with respect to local spherical neighborhoods of 3 μm radius. For the local cell density, the fraction of occupied cell volume in the local neighborhood was calculated. The local nematic order was computed as the average nematic order parameter $S = <3/2\ (\mathbf{n}_i\cdot\mathbf{n}_j)^2 - 1/2>$ in the local neighborhood, where $\mathbf{n}_i$ is the orientation vector of the focal cell and $\mathbf{n}_j$ are the orientation vectors of cells in the local neighborhood. One imaging location within a microfluidic channel was defined as one replicate. Three to five locations were imaged per channel.

Scanning electron microscopy of curli fibers

To visualize *in vitro* polymerized CsgA curli fibers *via* electron microscopy, curli fibers were deposited onto a poly-L-lysine coated glass slide for 1 h. Afterwards the fibers were fixed for 5 min with 4% paraformaldehyde, washed three times in dH$_2$O (each 5 min) and dehydrated in a graded ethanol series followed by critical point drying. Samples were sputter coated with platinum and imaged using a scanning electron microscope (JOEL JSM 7500-F). In order to visualize T7 phages bound to *in vitro* polymerized curli fibers, both were incubated together for 1 h under constant shaking. Unbound phages were removed *via* centrifugation (13000 rpm, 3 min) and washing of the curli fiber pellet with PBS was performed before deposition of the sample onto the poly-L-lysine coated glass slide. Preparation of samples involving curli fibers and beads required incubation of beads with pre-formed curli in the presence of 1% BSA for one hour under constant shaking before placing the bead-curli mixture on a poly-L-lysine coated glass slide.

Data availability

Raw as well as analyzed data that support the findings of this study are available from the corresponding authors upon request.

Supplementary Material

Refer to Web version on PubMed Central for supplementary material.

Acknowledgements

References

1. Flemming H-C, et al. Biofilms: an emergent form of bacterial life. Nat Rev Microbiol. 2016; 14:563–75. [PubMed: 27510863]

2. Persat A, et al. The mechanical world of bacteria. Cell. 2015; 161:988–97. [PubMed: 26000479]

3. Hobley L, Harkins C, MacPhee CE, Stanley-Wall NR. Giving structure to the biofilm matrix: an overview of individual strategies and emerging common themes. FEMS Microbiol Rev. 2015; 39:649–69. [PubMed: 25907113]

4. Berk V, et al. Molecular architecture and assembly principles of Vibrio cholerae biofilms. Science. 2012; 337:236–9. [PubMed: 22798614]

5. Drescher K, et al. Architectural transitions in Vibrio cholerae biofilms at single-cell resolution. Proc Natl Acad Sci U S A. 2016; 113:E2066–72. [PubMed: 26933214]

6. Nadell CD, Drescher K, Wingreen NS, Bassler BL. Extracellular matrix structure governs invasion resistance in bacterial biofilms. ISME J. 2015; 9:1700–9. [PubMed: 25603396]

7. Ochman H, Moran NA. Genes lost and genes found: evolution of bacterial pathogenesis and symbiosis. Science. 2001; 292:1096–9. [PubMed: 11352062]

8. Samson JE, Magadán AH, Sabri M, Moineau S. Revenge of the phages: defeating bacterial defences. Nat Rev Microbiol. 2013; 11:675–87. [PubMed: 23979432]

9. Zeng L, et al. Decision making at a subcellular level determines the outcome of bacteriophage infection. Cell. 2010; 141:682–91. [PubMed: 20478257]

10. Salmond GPC, Fineran PC. A century of the phage: past, present and future. Nat Rev Microbiol. 2015; 13:777–86. [PubMed: 26548913]

11. Rohwer F, Segall AM. In retrospect: A century of phage lessons. Nature. 2015; 528:46–8. [PubMed: 26632584]

12. Hu B, Margolin W, Molineux IJ, Liu J. The Bacteriophage T7 Virion Undergoes Extensive Structural Remodeling During Infection. Science (80-.). 2013; 339:576–579.

13. Koskella B, Brockhurst MA. Bacteria-phage coevolution as a driver of ecological and evolutionary processes in microbial communities. FEMS Microbiol Rev. 2014; 38:916–31. [PubMed: 24617569]

14. Gómez P, Buckling A. Bacteria-phage antagonistic coevolution in soil. Science. 2011; 332:106–9. [PubMed: 21454789]

15. Weitz JS, Hartman H, Levin SA. Coevolutionary arms races between bacteria and bacteriophage. Proc Natl Acad Sci U S A. 2005; 102:9535–40. [PubMed: 15976021]

16. Forde SE, et al. Understanding the limits to generalizability of experimental evolutionary models. Nature. 2008; 455:220–3. [PubMed: 18784724]

17. Bull JJ, Otto G, Molineux IJ. In vivo growth rates are poorly correlated with phage therapy success in a mouse infection model. Antimicrob Agents Chemother. 2012; 56:949–54. [PubMed: 22106213]

18. Chan BK, Abedon ST. Bacteriophages and their enzymes in biofilm control. Curr Pharm Des. 2015; 21:85–99. [PubMed: 25189866]

19. Doolittle MM, Cooney JJ, Caldwell DE. Tracing the interaction of bacteriophage with bacterial biofilms using fluorescent and chromogenic probes. J Ind Microbiol. 1996; 16:331–41. [PubMed: 8987490]

20. Lu TK, Collins JJ. Dispersing biofilms with engineered enzymatic bacteriophage. Proc Natl Acad Sci U S A. 2007; 104:11197–202. [PubMed: 17592147]

21. Briandet R, et al. Fluorescence correlation spectroscopy to study diffusion and reaction of bacteriophages inside biofilms. Appl Environ Microbiol. 2008; 74:2135–43. [PubMed: 18245240]

22. May T, Tsuruta K, Okabe S. Exposure of conjugative plasmid carrying Escherichia coli biofilms to male-specific bacteriophages. ISME J. 2011; 5:771–5. [PubMed: 20962879]

23. Vilas Boas D, et al. Discrimination of bacteriophage infected cells using locked nucleic acid fluorescent in situ hybridization (LNA-FISH). Biofouling. 2016; 32:179–90. [PubMed: 26813295]

24. Serra DO, Richter AM, Klauck G, Mika F, Hengge R. Microanatomy at cellular resolution and spatial order of physiological differentiation in a bacterial biofilm. MBio. 2013; 4:e00103–13. [PubMed: 23512962]

25. DePas WH, et al. Iron induces bimodal population development by Escherichia coli. Proc Natl Acad Sci U S A. 2013; 110:2629–34. [PubMed: 23359678]

26. Grantcharova N, Peters V, Monteiro C, Zakikhany K, Römling U. Bistable expression of CsgD in biofilm development of Salmonella enterica serovar typhimurium. J Bacteriol. 2010; 192:456–66. [PubMed: 19897646]

27. Pesavento C, et al. Inverse regulatory coordination of motility and curli-mediated adhesion in Escherichia coli. Genes Dev. 2008; 22:2434–46. [PubMed: 18765794]

28. Besharova O, Suchanek VM, Hartmann R, Drescher K, Sourjik V. Diversification of Gene Expression during Formation of Static Submerged Biofilms by Escherichia coli. Front Microbiol. 2016; 7:1568. [PubMed: 27761132]

29. Reyes A, Semenkovich NP, Whiteson K, Rohwer F, Gordon JI. Going viral: next-generation sequencing applied to phage populations in the human gut. Nat Rev Microbiol. 2012; 10:607–17. [PubMed: 22864264]

30. Pires DP, Oliveira H, Melo LDR, Sillankorva S, Azeredo J. Bacteriophage-encoded depolymerases: their diversity and biotechnological applications. Appl Microbiol Biotechnol. 2016; 100:2141–51. [PubMed: 26767986]

31. Arnqvist A, Olsén A, Pfeifer J, Russell DG, Normark S. The Crl protein activates cryptic genes for curli formation and fibronectin binding in Escherichia coli HB101. Mol Microbiol. 1992; 6:2443–52. [PubMed: 1357528]

32. Olsén A, Jonsson A, Normark S. Fibronectin binding mediated by a novel class of surface organelles on Escherichia coli. Nature. 1989; 338:652–5. [PubMed: 2649795]

33. Zhou Y, Smith DR, Hufnagel DA, Chapman MR. Experimental manipulation of the microbial functional amyloid called curli. Methods Mol Biol. 2013; 966:53–75. [PubMed: 23299728]
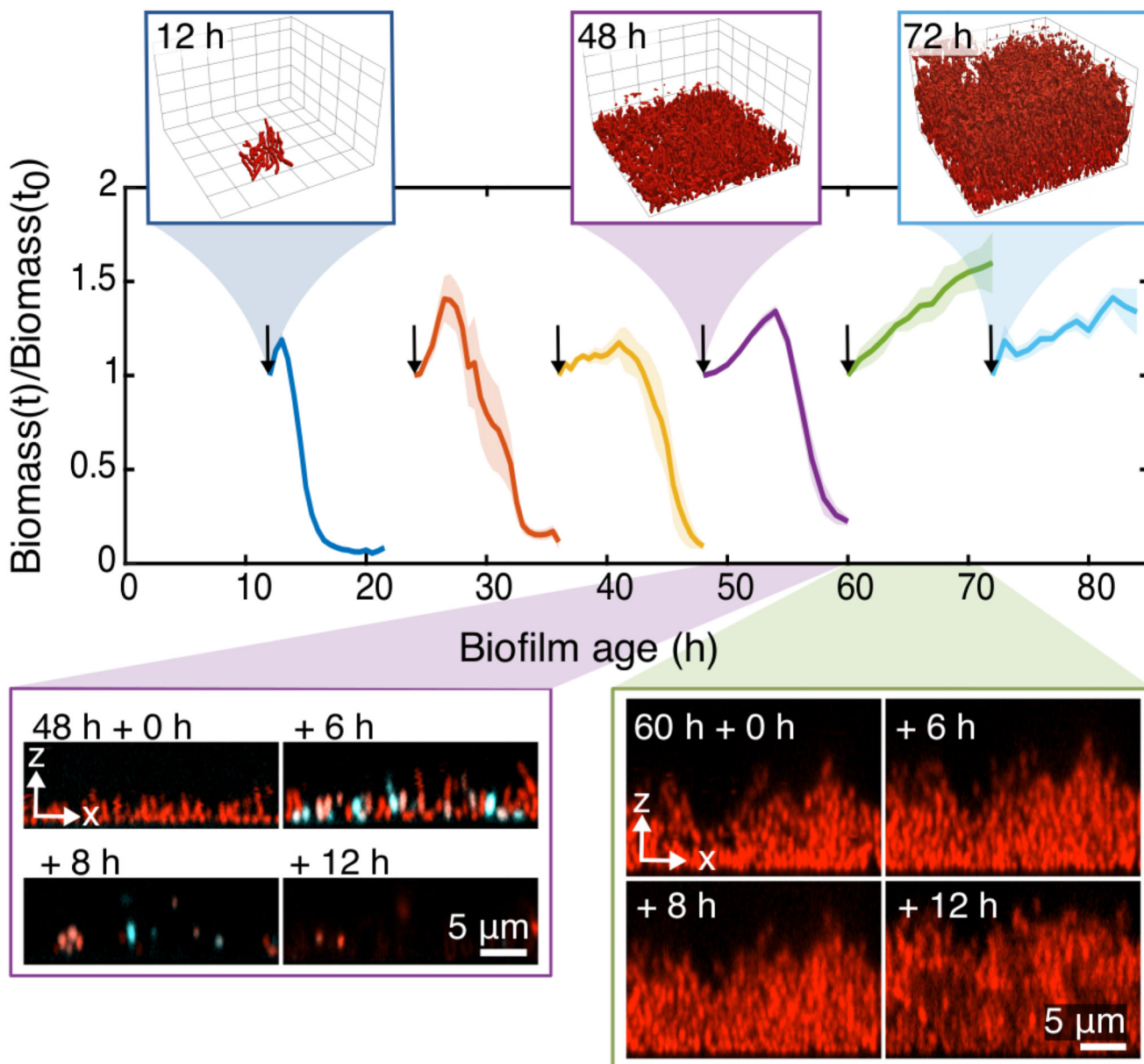
**Figure 1. Susceptibility of biofilms to phage exposure as a function of biofilm age.**
Lines denote the mean biofilm biomass at time t, normalized by the biomass at the time of phage exposure t_0, and shaded areas denote the standard error of the mean (t_{12h} n=8; t_{24h} n=10; t_{36h} n=3; t_{48h} n=4; t_{60h} n=4; t_{72h} n=7). Note that in some cases, the standard error is narrower than the line denoting the mean value. Arrows at the start of each curve denote the introduction of phages to the system, and different colored curves represent different biofilm ages at first phage exposure. Young biofilms were destroyed by propagating waves of phage infection and host cell lysis. Biofilms older than 60 h showed little phage infection and continued to increase in size despite the continuous flux of phages across the biofilms. In the bottom panels, red cells are uninfected, and phage-infected cells are cyan, due to a phage-encoded green fluorescent protein.
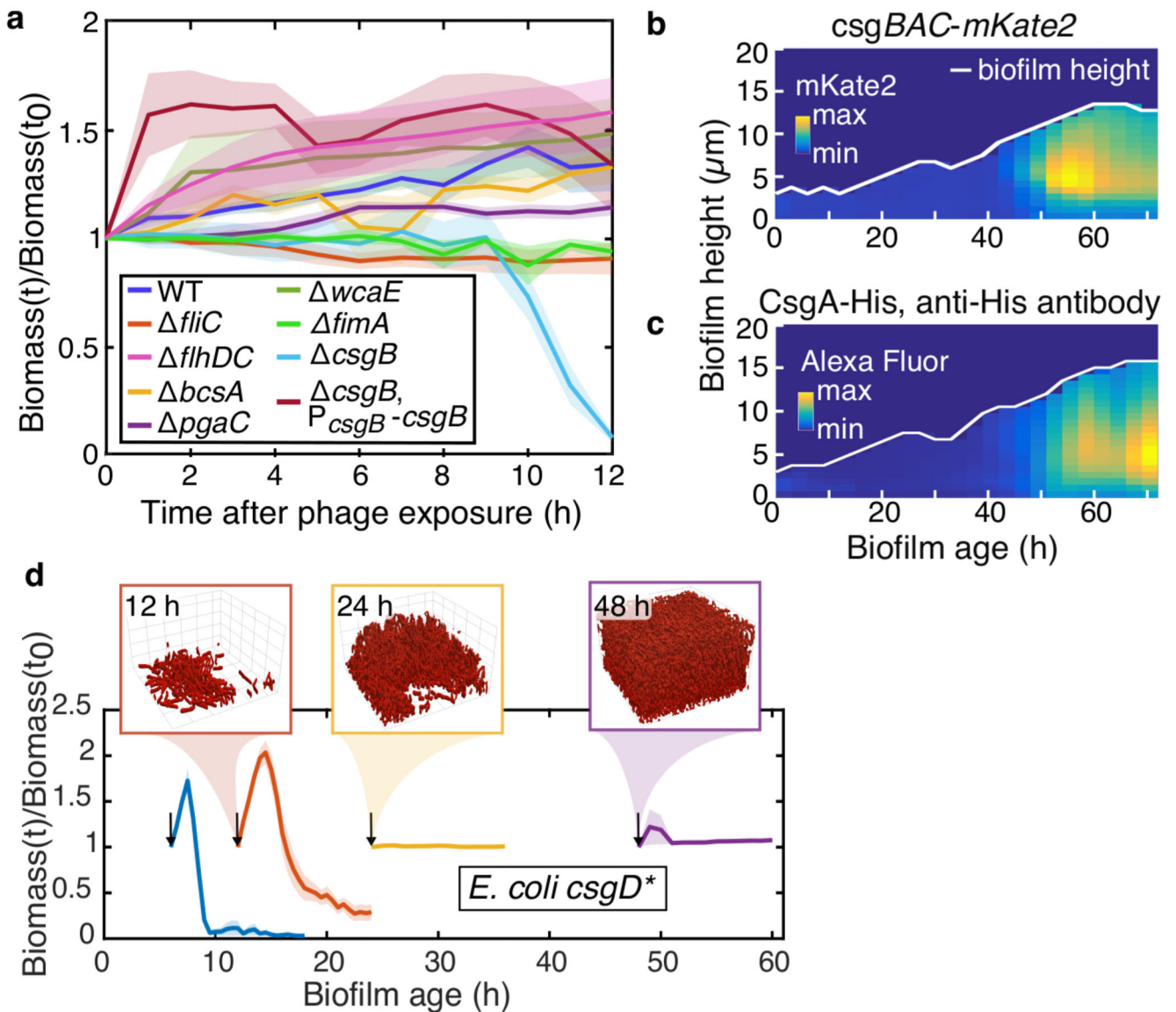
Figure 2. Phage susceptibility of biofilms depends on extracellular matrix structure and dynamics.

a, Biofilm susceptibility was assayed after 72 h of normal biofilm development. Mutants deficient in *csgB*, which is required to nucleate curli polymers, are susceptible to phage epidemics regardless of biofilm age, whereas mutants lacking one of the other major matrix components remain protected against phages (*fliC*: flagellin; *flhDC:* flagellar master regulator; *bcsA*: cellulose; *pgaC*: poly-β-1,6-*N*-acetyl-D-glucosamine; *wcaE*: colanic acid; *fimA*: type 1 fimbriae). Phage protection can be complemented with ectopic expression of *csgB*. Lines denote the mean biofilm biomass and shaded areas denote the standard error of the mean (n_{fliC}=3; n_{flhDC}=5; n_{bcsA}=4; n_{pgaC}=5; n_{wcaE}=5; n_{fimA}=3; n_{csgB}=3; $n_{csgB,PcsgB-csgB}$=3). **b**, Spatiotemporal dynamics of transcription of the *csgBAC* operon, using an *mKate2*-based reporter (*n*=4), and **c** deposition of curli polymers into the extracellular matrix, using a fluorescent antibody to CsgA-His (*n*=3). **d**, Biofilms of cells

harboring a *csgD** promoter mutation, which yields an overexpression of biofilm matrix (including curli polymers), display phage protection after ~24 h of biofilm growth, consistent with the prediction that early production of curli shifts the time window at which biofilms can withstand phage exposure. *csgD** biofilms at 24h and 48h are alive, but grow slowly. Lines denote the mean biofilm biomass and shaded areas denote the standard error of the mean (t_{6h} n=4; t_{12h} n=8; t_{24h} n=7; t_{48h} n=6).
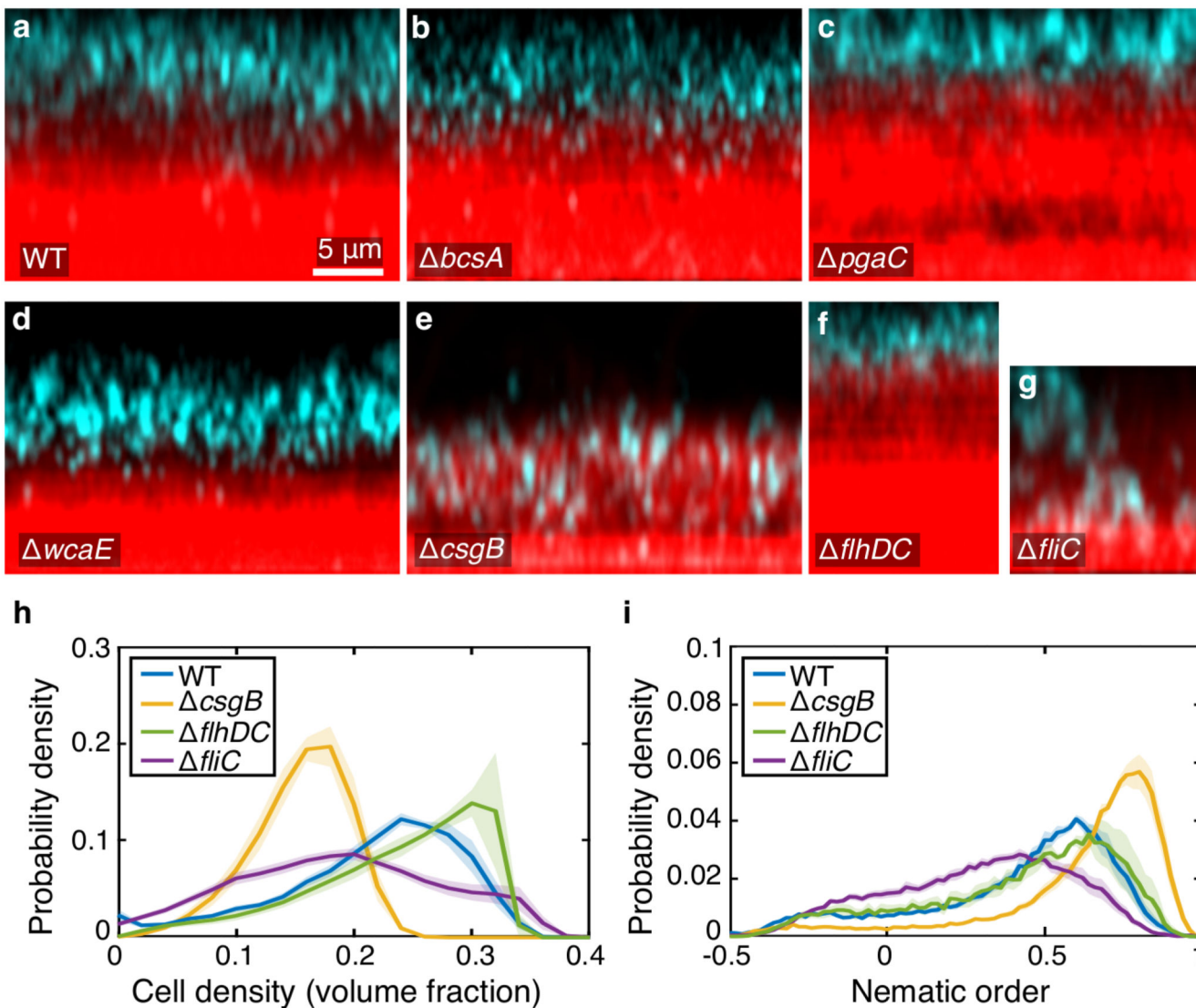
Figure 3. Phage localization and biofilm architectural properties within wild type E. coli and mutants lacking major extracellular matrix components.

Panels **a-g** show maximum intensity *z*-projections of 72-h old biofilms after 8 h of phage exposure. The scale bar in panel **a** applies to all panels **a-g**. Cells are labeled red and phage particles are labeled cyan. For biofilms of **a** wild type cells (*n*=4) and mutants lacking **b** cellulose (*n*=3), **c** poly-β-1,6-*N*-acetyl-D-glucosamine (*n*=3), **d** colanic acid (*n*=6) or **f** the flagellar master regulator (*n*=7), phages could be observed only on the outer periphery of 72-h old biofilms. For mutants lacking **e** curli fibers (*n*=4) or **g** flagellin (*n*=7), however, phages could readily diffuse through the biofilms. **h,** Single-cell resolution analysis of the biofilm architecture showed that *csgB* and *fliC* mutants produce less densely-packed biofilms than wild type cells or *flhDC*. **i,** Biofilms lacking curli fibers showed higher cell-cell alignment, measured in terms of the nematic order parameter, whereas *fliC* showed lower cell-cell alignment, compared with wild type biofilms. The cell-cell alignment within *flhDC* biofilms resembled the one observed for wild type biofilms. Lines denote means and

shaded areas denote the standard error of the mean (n_{WT} =9; n_{csgB} =9; n_{flhDC} =5; n_{fliC} =24).
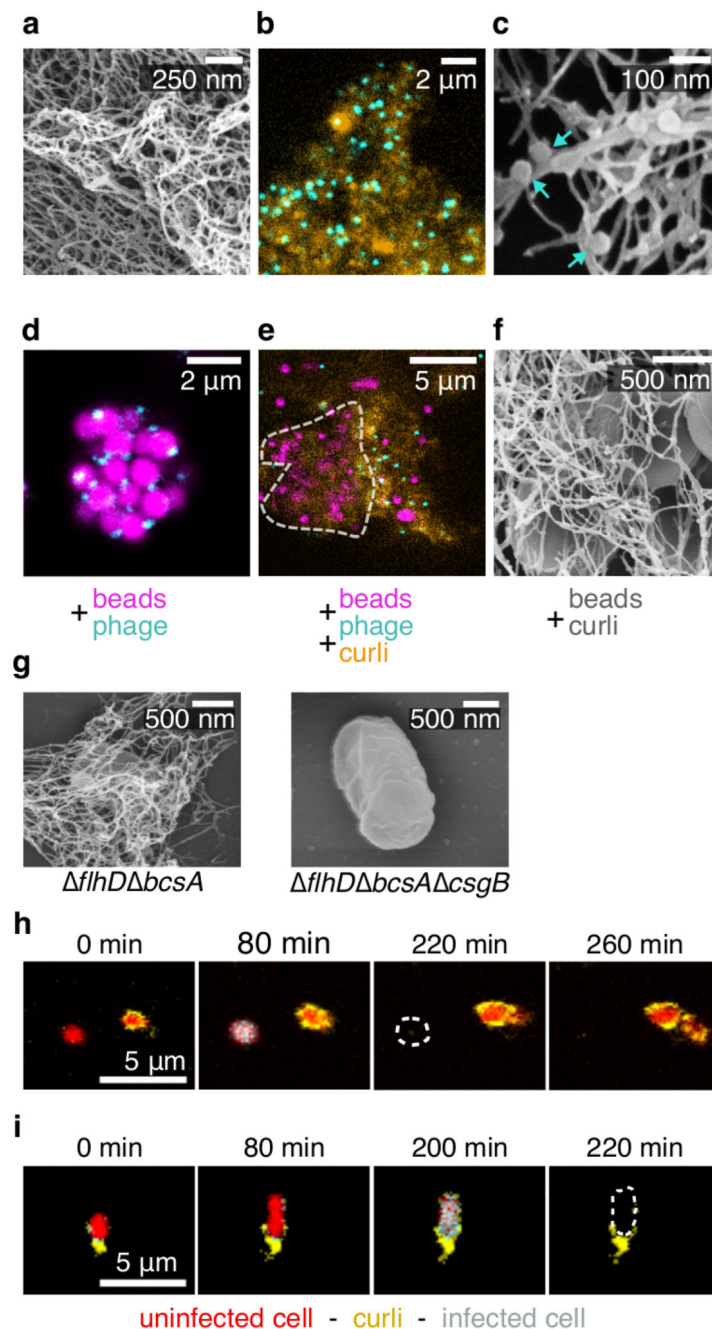
Figure 4. Reconstruction of minimal synthetic biofilms recapitulates phage diffusion prevention and phage-cell attachment prevention *in vivo*.

a, The curli fiber monomer CsgA was purified and shown by electron microscopy to polymerize *in vitro* (*n*=2). **b**, Curli fibers alone, visualized by immunostaining (orange), permit free diffusion of phage virions (cyan) into the curli mesh (*n*=3). **c**, Phages can bind to curli fibers that were polymerized *in vitro* before phage exposure, as indicated by the arrows (*n*=3). **d**, Fluorescent beads (magenta) were used as artificial replacements for bacterial cells. 1 μm diameter beads permit diffusion of phage virions throughout the interior of bead

clusters. **e**, When beads are combined with curli polymers to produce minimal artificial biofilms, the bead clusters were protected from phage diffusion (*n*=4). **f**, Preformed curli fibers, when incubated with beads, localize between individual beads and wrap around bead clusters as shown by electron microscopy (*n*=3). **g,** Individual cells that are capable of curli production (but incapable of flagella and cellulose production) embed themselves in a dense mesh made out of self-produced curli fibers (*n*=3). **h**, Individual bacteria (red) that are surrounded by curli (yellow) are not infected by phages and can divide normally, whereas cells that are not surrounded by curli become infected (grey), and then lyse (white dashed line) (*n*=5). **i**, Bacteria that are not completely surrounded by curli are not protected from phage infection (*n*=5).